NEUROSCIENCE

Mechanosensory circuits coordinate two opposing motor actions in *Drosophila* feeding

Yao Zhou[1,2,3,4]*, Li-Hui Cao[1,2,3,4,5]*, Xiu-Wen Sui[5], Xiao-Qing Guo[1,2,3,4], Dong-Gen Luo[1,2,3,4,5]†

Mechanoreception detects physical forces in the senses of hearing, touch, and proprioception. Here, we show that labellar mechanoreception wires two motor circuits to facilitate and terminate *Drosophila* feeding. Using patch-clamp recordings, we identified mechanosensory neurons (MSNs) in taste pegs of the inner labella and taste bristles of the outer labella, both of which rely on the same mechanoreceptor, NOMPC (no mechanoreceptor potential C), to transduce mechanical deflection. Connecting with distinct brain motor circuits, bristle MSNs drive labellar spread to facilitate feeding and peg MSNs elicit proboscis retraction to terminate feeding. Bitter sense modulates these two mechanosensory circuits in opposing manners, preventing labellar spread by bristle MSNs and promoting proboscis retraction by peg MSNs. Together, these labeled-line circuits enable labellar peg and bristle MSNs to use the same mechanoreceptors to direct opposing feeding actions and differentially integrate gustatory information in shaping feeding decisions.

INTRODUCTION

Feeding is critical for survival and reproduction. The decision of whether to eat is affected by both the chemical and physical properties of food, and mouthparts are equipped with a set of sensory neurons to evaluate these features. The roles of contact chemoreception or gustation in detecting the chemical composition of food have been well studied (*1*–*4*). In both *Drosophila* and mammals, sweet and bitter are detected by distinct gustatory receptors, whose activation elicits taste acceptance and avoidance behaviors, respectively (*5*). In contrast, how physical features of food affect feeding is just beginning to be illustrated (*6*–*8*). In principle, mouth mechanoreception is able to evaluate food before and during ingestion, providing information about food availability, location, and texture. Mechanosensory neurons (MSNs) are known to innervate different mouthparts, such as the lips and tongue (*9*), but whether and how the MSNs in different mouthparts play distinct roles in feeding remain unclear.

After encountering a food source, a hungry fly sequentially stops walking, extends its proboscis, spreads its labellar lobes, sucks food, and then retracts its proboscis (*10*). The molecular and circuit basis underlying some of these feeding events has been elucidated (*11*–*15*). A *Drosophila* labellum has 31 taste bristles and 35 pegs, each of which contains one to four gustatory receptor neurons (GRNs) in addition to an MSN (*1*, *2*). In total, there are approximately 130 MSNs in the two labella (*16*). Recently, NANCHUNG-expressing (*6*) and no mechanoreceptor potential C (NOMPC)–expressing labellar neurons (*7*) have been reported to detect food texture. In addition, transmembrane-like channel (TMC) protein-expressing multidendritic neurons in the labella have also been reported to detect food texture (*8*). However, the neural circuits and synaptic mechanisms underlying their feeding control remain unknown. In addition, whether and how the 130 labellar MSNs in taste pegs and bristles play different roles in feeding remain unknown. Here, we address the following three questions of mechanoreception in *Drosophila* feeding: (i) whether and how peg and bristle MSNs detect different food features, (ii) whether and how peg and bristle MSNs direct distinct feeding behaviors, and (iii) how peg and bristle MSNs integrate gustatory information to shape feeding decisions.

Here, by combining patch-clamp recordings, optogenetic tools, circuitry tracing, and behavioral studies, we investigated the circuit basis underlying mouth mechanoreception in *Drosophila* feeding. We found that mechanoreception rather than chemoreception controls labellar spread during feeding. By developing patch-clamp recordings on *Drosophila* MSNs, we identified the taste peg MSNs and found that they, as well as bristle MSNs, rely on the mechanotransduction channel, NOMPC, in mechanoelectrical transduction. Our circuitry tracing revealed that peg MSNs and bristle MSNs wire two distinct feeding circuits. Optogenetic activation of bristle MSNs elicited labellar spread, while activation of peg MSNs drove proboscis retraction. Notably, these two mechanically driven behaviors were oppositely regulated by bitter sensation. Therefore, the labeled-line wiring of labellar mechanoreception enables the fly to control two distinct feeding circuits using a single type of mechanosenstive channel.

RESULTS

Mechanical stimuli trigger labellar spread

During natural feeding, *Drosophila* shows stereotypical and sequential motor actions (*11*). The two labellar lobes remain closed during proboscis extension and open only upon food contact (Fig. 1A and movie S1). The interval between food contact and the start of labellar spread could be as short as 10 ms (fig. S1, A and B). Similarly, in induced feeding, labellar spread occurred after the labella, but not the legs, contacted a sugar solution (fig. S1, C and D, and movie S2).

Next, we investigated the sensory stimulus that elicits labellar spread. In blowflies, the activation of sugar-sensing neurons has been suggested to produce labellar spread (*17*). To test this possibility, we

[1]State Key Laboratory of Membrane Biology, College of Life Sciences, Peking University, Beijing 100871, China. [2]PKU-IDG/McGovern Institute for Brain Research, Peking University, Beijing 100871, China. [3]Peking-Tsinghua Center for Life Sciences, Academy for Advanced Interdisciplinary Studies, Peking University, Beijing 100871, China. [4]College of Life Sciences, Peking University, Beijing 100871, China. [5]Center for Quantitative Biology, Academy for Advanced Interdisciplinary Studies, Peking University, Beijing 100871, China.
*These authors contributed equally to this work.
†Corresponding author. Email: dgluo@pku.edu.cn

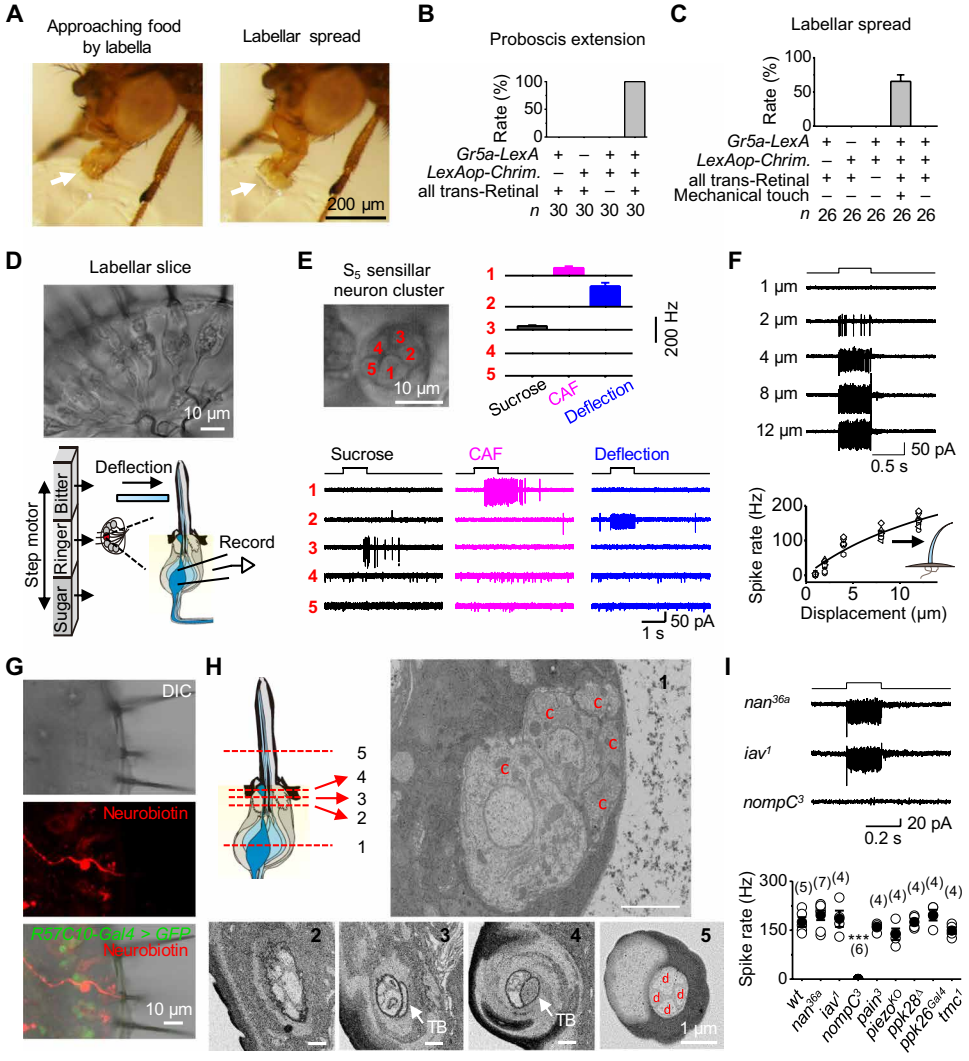

Fig. 1. Labellar spread and mechanical detection by taste bristles. (**A**) Labellar spread during natural feeding. The extended labella approach the food with two labellar lobes closed (left, arrow), followed by opening of the two labellar lobes upon food contact (right, arrow). (**B**) Sweet gustation does not drive labellar spread. Optogenetic activation of the *CsChrimson*-expressing *Gr5a*-GRNs produces proboscis extension but does not elicit labellar spread. Light stimulation: 1 s, 617 nm. (**C**) Mechanical stimulation drives labellar spread. Optogenetic activation of *Gr5a*-GRNs elicits proboscis extension; labellar lobes spread apart upon touching a coverslip. Light stimulation: 1 s, 617 nm. (**D**) A labellar slice preparation. Top: Differential interference contrast (DIC) image of a labellar slice. Bottom: Gustatory stimulation (left); mechanical stimulation and single-cell suction-pipette recordings on a sensory neuron (right). (**E**) Sensory responses of the S_5 sensillar neurons. Top: DIC image of five neurons in one S_5 sensillum (left); collective data of spike responses of the five neurons averaged across different S_5 sensilla, in which all five neurons are recorded successfully one by one (right; $n = 6$). Bottom: Spike responses of individual neurons in one S_5 sensillum to mechanical deflection (10 μm) and gustatory stimuli [50 mM caffeine (CAF) and 100 mM sucrose]. (**F**) Deflection dependence of mechanosensory responses. Top: Spike responses to sensillar deflection. Bottom: Collective data ($n = 8$). The fit is with a Boltzmann function. (**G**) Bristle MSNs do not extend dendrites into the bristle cavity. Top: DIC image of a labellar slice. Middle: Neurobiotin labeling of a mechanosensitive neuron. Bottom: Overlay of the DIC, green fluorescent protein (GFP), and neurobiotin images. *GMR57C10-Gal4* is a pan-neuron driver. (**H**) Structure of sensory neurons in a bristle by electron microscopy. Top: Illustration of five positions (left); the five neuronal cell bodies of the same bristle at position 1 (right). Bottom: Five dendrites of the bristle at position 2; four dendrites and one tubular body at position 3; the large tubular body at position 4; four dendrites and no tubular body in one sensillar cavity at position 5. c, cell body; TB, tubular body; d, dendrite. (**I**) NOMPC-dependent mechanosensitivity. Top: Representative spike responses to sensillar deflection. Bottom: Collective data of firing rates (calculated as five times the total spikes during the 200-ms deflection). Mechanical deflection, 200 ms and 10 μm. ***$P < 0.001$. wt, wild-type.

expressed an excitatory light-gated ion channel, *CsChrimson* (*18*), in all sugar-sensing neurons with a *Gr5a-LexA* driver. In starved flies, optogenetic activation of the labella triggered extension of the proboscis (Fig. 1B and movie S3). However, the two labellar lobes remained closed, although the proboscis was fully extended (Fig. 1C and movie S3), demonstrating that the activation of sugar-sensing neurons was not sufficient to drive labellar spread.

Alternatively, the opening of labellar lobes may be driven by mechanical signals when the labellum contacts food. To examine this possibility, we mounted a food-free coverslip in front of the proboscis to provide mechanical contact. The starved fly extended its proboscis after optogenetic activation of sugar-sensing neurons, and its two labellar lobes immediately spread out when the labella touched the coverslip (Fig. 1C and movie S4). These results demonstrated that

mechanical signals elicit the opening of the two labellar lobes, and these signals were likely detected by MSNs in the bristles of the outer labellar surface.

Physiology of MSNs in taste bristles

To search for bristle MSNs that detect mechanical force, we performed single-cell suction-pipette recordings (*19*) of sensory neurons in taste bristles of a labellar slice preparation that we developed (Fig. 1D). In this preparation, taste bristles remained intact, thus maintaining the sensory transduction mechanisms of both gustation and mechanoreception. Unlike the *Drosophila* peripheral olfactory system (*20*), labellar neurons are grouped into distinct and physically separate clusters for each bristle, with each cluster containing three or five neurons (Fig. 1D). After removing the sheath cells that wrap the neuronal cell bodies, we drew one cell body into a recording pipette. A loose seal between the pipette and cell body allowed us to record spike activity of the cell (Fig. 1D). This single-cell recording method maintained neuronal integrity without dialysis of intracellular signaling molecules (*19*), thus enabling a stable, long-lasting recording (>1 hour). For mechanical stimulation, we deflected the sensillum with a glass pipette that was driven by a piezo actuator (Fig. 1D). For gustatory stimulation, we used a fast solution change system (*20*).

Taste bristles are categorized into short (S), intermediate (I), and long (L) types of sensilla (*1*, *2*). To characterize all sensory neurons in a single sensillum, we recorded them one by one. Among the five neurons of the S_5 sensillum, we found that one responded to sensillar deflection by firing a train of action potentials (Fig. 1E). This deflection-sensitive neuron did not respond to gustatory stimulation of sucrose or caffeine (CAF). Similar mechanosensitive neurons were found in other S-, I-, and L-type sensilla (fig. S2, A to C). We also found two other neurons that responded to sucrose or CAF, but neither responded to sensillar deflection (Fig. 1E).

As expected, the firing frequency of action potentials increased with sensillar deflection (Fig. 1F). To examine the anatomical features of these deflection-sensitive neurons, we injected neurobiotin into them via whole-cell recording pipettes. The neurobiotin diffused from the pipette to the cell, revealing a dendritic termination below the sensillar socket (Fig. 1G), which differed from the dendritic ending within the sensilla by chemosensory neurons (fig. S2D). To further examine the fine structure of bristle MSNs, we performed morphological studies with electron microscopy. The bristle examined had five neurons, four of which extended their dendrites into the sensillum (Fig. 1H). The dendrite of the fifth neuron became a tubular body and terminated below the sensillar socket (Fig. 1H and movie S5), a key feature of labellar MSNs (*21*).

Several mechanosensitive channels, including the epithelial sodium channel [encoded by the *pickpocket* (*PPK*) gene], the transient receptor potential channel (TRPs: NANCHUNG, INACTIVE, NOMPC, and PAINLESS), the PIEZO channel, and the TMC, have been identified in *Drosophila* (*8*, *22*–*29*). To identify the channels that mediate mechanotransduction of bristle MSNs, we screened flies with ablated candidate channels for impaired electrical responses to sensillar deflection. We found that the spike firing to mechanical stimulations was intact in nan^{36a}, iav^{1}, $pain^{3}$, $piezo^{KO}$, $ppk28^{\Delta}$, $ppk26^{Gal4}$, and tmc^{1} mutants (Fig. 1I). In contrast, the deflection-induced spike firing was completely eliminated in $nompC^{3}$ flies (Fig. 1I), consistent with the finding that NOMPC was required for the mechanosensitivity of labellar MSNs on the basis of field potential recordings of taste bristles (*7*).

Mechanoelectrical transduction by bristle MSNs

To study the mechanoelectrical transduction of bristle MSNs, we examined whether they could be identified by driver lines for patch-clamp recordings. We found that, among the many published lines, *nompC-QF*, *nompC-LexA*, and *GMR41E11-Gal4* labeled many neurons in the labellum (Fig. 2A, fig. S3A, and table S1), with the latter two reported to label labellar MSNs (*6*, *7*). Green fluorescent protein (GFP)–labeled neurons by the *nompC-QF*, *nompC-LexA*, and *GMR41E11-Gal4* lines extended their dendrites below the labellar cuticle (Fig. 2A and fig. S3A), a unique feature of bristle MSNs (Fig. 1G). To examine whether these neurons were mechanosensitive, we performed single-cell suction-pipette recordings and found that these neurons responded robustly to sensillar deflection but did not respond to gustatory stimuli (Fig. 2B and fig. S3B), consistent with previous findings (*6*, *7*). Therefore, the bristle neurons labeled by *nompC-QF*, *nompC-LexA*, and *GMR41E11-Gal4* were bona fide MSNs in taste bristles. Their spike firing induced by sensillar deflection was completely eliminated in $nompC^{3}$ flies and was restored (Fig. 2C) by rescuing the expression of a long form of NOMPC (*30*).

Next, we performed patch-clamp recordings on these GFP-labeled bristle MSNs to study their cellular mechanotransduction properties. Under current clamp, a brief sensillar deflection triggered a depolarization accompanied by action potential firing (Fig. 2D). Furthermore, a sensillar deflection triggered inward mechanotransduction receptor currents under a voltage-clamp configuration (Fig. 2E, top), with a response delay of approximately 3 ms (Fig. 2E, bottom). To gain further insight into mechanotransduction channels, we examined their current-voltage (I-V) relationship. Within a voltage range between −75 mV and +65 mV, the I-V relationship of mechanotransduction currents in native MSNs was linear with a reversal potential of 7 ± 1 mV (Fig. 2F), consistent with the channel properties of NOMPC examined in the heterologous expression system of S2 cells (*25*). Therefore, the mechanotransduction currents in bristle neurons were mediated by nonselective cation channels.

With the ability to directly record the mechanotransduction receptor currents of *Drosophila* MSNs for the first time, we examined whether NOMPC played roles in transduction (*28*, *31*) or simply in amplification of the signals (*32*). We found that the mechanotransduction currents were completely abolished in $nompC^{3}$ flies (Fig. 2, G and H), consistent with a direct role for NOMPC in mechanotransduction (*28*, *31*). In contrast, the mechanotransduction currents remained intact in the nan^{36a} and iav^{1} mutant flies (Fig. 2, G and H). The bristle MSNs of $nompC^{3}$ flies, compared with those of control flies, produced similar depolarization in response to current injections (fig. S3C), thus implying that the loss of mechanotransduction currents was not due to a general impairment of neuronal excitability. In addition, the loss of mechanotransduction currents in $nompC^{3}$ flies was restored by rescuing NOMPC (Fig. 2, G and H).

Physiology of peg MSNs

In addition to taste bristles, approximately 35 taste pegs are located in the inner surface of each labellar lobe (*21*). Taste pegs are short (~3 μm) and covered by a fold (Fig. 3A), and each contains two sensory neurons, one of which is assumed to be chemosensitive and the other mechanosensitive (*2*, *21*). However, the nature of the mechanosensitive responses and physiological functions of peg MSNs remain unknown due to the difficulty in their access by recording electrodes. With a membrane GFP reporter, we found that the *NP7506-Gal4* driver labeled only one neuron in each taste peg

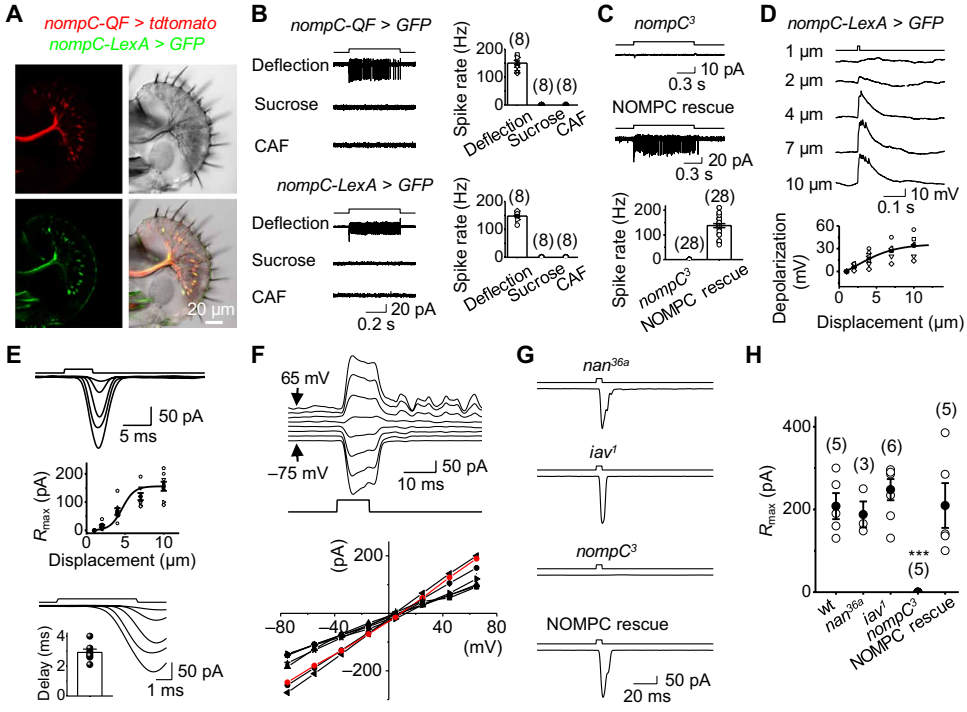

Fig. 2. Mechanoelectrical transduction of bristle MSNs. (**A**) Images of a labellar slice with coexpression of tdtomato by *nompC-QF* (top left) and GFP by *nompC-LexA* (bottom left), DIC image of the labellar slice (top right), and overlay of DIC, tdtomato, and GFP channels (bottom right). (**B**) Mechanosensitivity of NOMPC-expressing bristle neurons. Top: Spike responses of the bristle neuron labeled by *nompC-QF* to gustatory and mechanical stimuli (left); collective data (right). Bottom: Spike responses of the bristle neuron labeled by *nompC-LexA* (left); collective data (right). Mechanical deflection, 10 μm; sucrose, 100 mM; CAF, 50 mM. (**C**) NOMPC is required for mechanosensitivity. Top: The bristle neuron labeled by *nompC-LexA* lost spike responses to sensillar deflection in *nompC*^{3} flies. Middle: NOMPC rescue restores mechanosensitivity of the bristle neurons in *nompC*^{3} flies. Bottom: Collective data. Mechanical deflection, 10 μm. (**D**) Patch-clamp recordings of mechanosensory responses. The *nompC-LexA*–labeled bristle neuron is recorded under current-clamp configuration. Sensillar deflection produces graded depolarization and spike firing (top); collective data (bottom). The deflection amplitudes are indicated. The fit is with a Boltzmann function. $n = 6$. (**E**) Mechanotransduction currents. Top: Deflection-current response families under voltage-clamp configuration. Sensillar deflection: 1, 2, 4, 7, and 10 μm. Middle: Deflection-response relationship. The normalized peak amplitudes of mechanotransduction currents are plotted against the displacement. The curve fit is with a Boltzmann function: $R/R_{max} = 1/\{1\text{-exp}[-(X - X_{1/2})/X_{slope}]\}$, where R is the peak amplitude of mechanoreceptor currents, R_{max} is the maximum response, X is the displacement, $X_{1/2}$ is the displacement that half-saturates the responses, X_{slope} is the slope of the response curve, $X_{1/2} = 4.0 \pm 0.5$ μm ($n = 8$), and $X_{slope} = 2.1 \pm 0.6$ ($n = 8$). Bottom: Mechanotransduction currents are shown on an expanded time scale; inset is collective data ($n = 8$). (**F**) I-V relationship of mechanotransduction current. Top: Mechanotransduction currents at different voltages as indicated. The cell was voltage-clamped at −75 mV and then stepped to +65 mV in 20-mV increments. Mechanical deflection, 10 μm. Bottom: Collective data ($n = 8$). (**G**) NOMPC is required for mechanotransduction. *nompC*^{3} eliminates mechanotransduction currents; *nan*^{36a} and *iav*^{1} mutants do not affect the mechanotransduction currents. Mechanical deflection, 10 μm. (**H**) Collective data for (G). ***$P < 0.001$.

(Fig. 3B), which has been reported to be the MSN based on its axonal projection (*33*). To examine whether these peg neurons are mechanosensitive, we performed single-cell recordings on a labellar slice preparation that maintains peg structure but exposes the cell bodies of peg neurons (Fig. 3B). Under suction-pipette recordings, *NP7506*-labeled peg neurons produced robust action potential firing in response to mechanical deflection but did not respond to gustatory stimuli (Fig. 3C). The firing frequency increased with sensillar deflection (Fig. 3D). Similar to bristle MSNs, these peg neurons produced a fast inward mechanotransduction current that depolarized the cell to fire action potentials under patch-clamp recordings (Fig. 3E). Therefore, the *NP7506*-labeled peg neurons are also bona fide MSNs.

To identify the mechanosensitive channels in peg MSNs, we screened flies with ablated candidate channels for impaired electrical responses to peg deflection. We found that mechanically induced spike firing was intact in *nan*^{36a}, *iav*^{1}, *pain*^{3}, *piezo*^{KO}, *ppk28*$^{\Delta}$, *ppk26*^{Gal4}, and *tmc*^{1} mutants but was completely eliminated in *nompC*^{3} flies (Fig. 3F). The mechanotransduction currents were eliminated in *nompC*^{3} flies but remained intact in *nan*^{36a} flies (Fig. 3G), indicating that NOMPC mediates mechanotransduction in peg MSNs.

Two distinct feeding behaviors directed by labellar MSNs

The above results demonstrated that both bristle and peg MSNs rely on NOMPC for mechanotransduction. Next, we examined whether these two types of labellar MSNs project their axons to the same or different brain regions for central processing (Fig. 4A). To examine the axonal projection of peg MSNs, we generated flies with the genotype of *NP7506-Gal4*, *UAS-SYN21-GFP-P10*, labeling all peg MSNs in addition to two to four bristle MSNs (Fig. 4B, top). In the brain, intense GFP signals appeared in an axonal track in the anterodorsal subesophageal zone (SEZ), a known gustatory center (Fig. 4C, top). The *tdtomato* driven by *nompC-LexA* that labeled both bristle and peg MSNs (Fig. 4B, middle) also labeled the peg MSN track, in addition to a distinct SEZ region that was not targeted by peg MSNs (Fig. 4C, middle). This additional SEZ labeling may reflect the axonal projections of bristle MSNs. To examine this possibility, we performed specific labeling of bristle MSNs with the use of combination of genetic

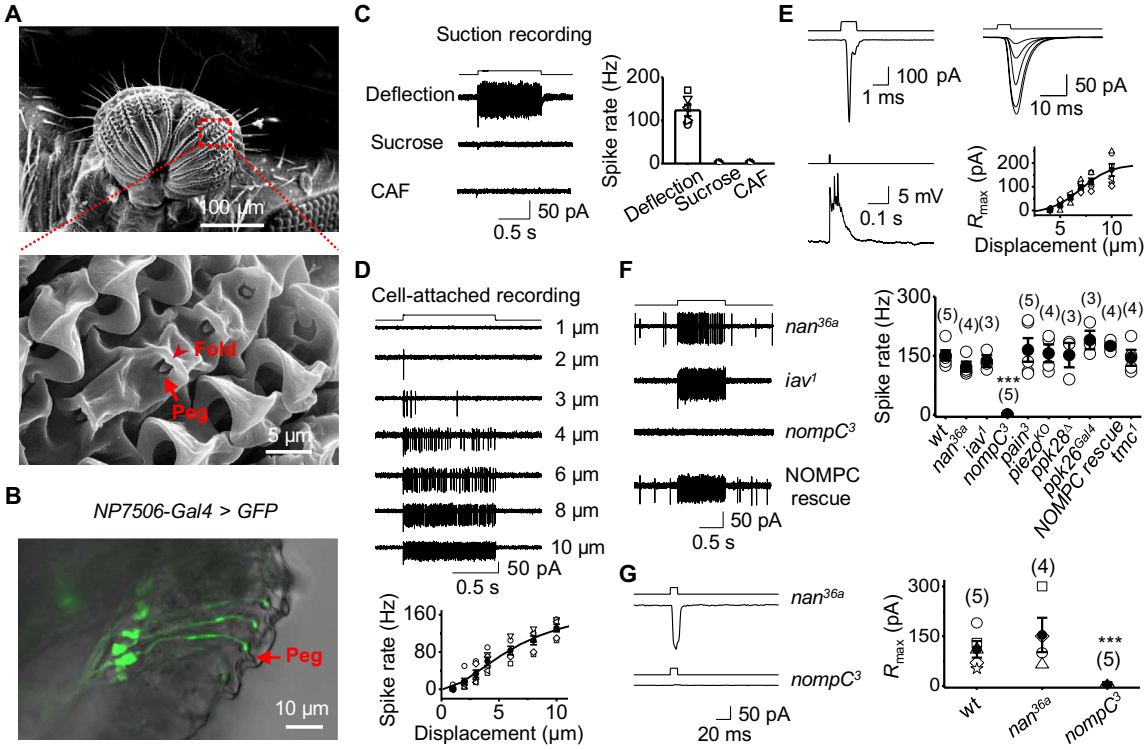

Fig. 3. Physiology of MSNs in taste pegs. (**A**) SEM image of taste pegs. The inner oral surface of two labellar lobes (top) with the boxed region further magnified (bottom). Taste pegs (arrow) are covered by a fold (arrowhead). (**B**) Peg neurons labeled by *NP7506-Gal4*. Overlap DIC and GFP images of a labellar slice from a *NP7506-Gal4*, *UAS-SYN21-GFP-P10* fly. The arrow indicates a peg. (**C**) Peg neurons labeled by *NP7506-Gal4* are mechanosensitive. The recorded *NP7506* peg neuron fires action potentials to peg deflection but not sucrose and CAF (left); collective data (right; $n = 6$). Mechanical deflection, 10 μm; sucrose, 100 mM; CAF, 50 mM. (**D**) Deflection dependence. Spike firing rate increases with peg deflection (top); collective data (bottom; $n = 6$). The fit is with a Boltzmann function. The deflection amplitudes are indicated. (**E**) Patch-clamp recordings on peg MSNs. Left: Mechanotransduction currents (deflection, 1 ms and 10 μm; voltage clamp, top); depolarization and action potential firing (current clamp, bottom). Right: A family of superimposed mechanotransduction currents to a 5-ms deflection of 4, 5, 6, 7, 8, and 10 μm (top); the current-displacement relationship (bottom) with $X_{1/2} = 7.0 \pm 0.1$ μm and $X_{slope} = 1.43 \pm 0.01$ ($n = 6$). (**F**) Dependence of mechanosensitivity of peg neurons on NOMPC. Left: Representative spike firing to sensillar deflection. Right: Collective data. ***$P < 0.001$. Mechanical deflection, 10 μm. (**G**) NOMPC is required for mechanotransduction. Left: *nompC*^{3} eliminates mechanotransduction currents; *nan*^{36a} does not affect mechanotransduction currents. Right: Collective data. Mechanical deflection, 10 μm. ***$P < 0.001$.

tools. We generated flies with the genotype of *nompC-LexA*, *LexAop-FRT-CsChrimson.mVenus-FRT*, which drives *CsChrimson.mVenus* expression in bristle MSNs but flips out the expression in peg MSNs with *NP7506-Gal4/UAS-FLP*. Because of the stochastic recombination of *FLP-FRT*, we found that bristle MSNs were exclusively labeled in 60 of 600 flies by *CsChrimson.mVenus* (Fig. 4B, bottom). In these flies, the SEZ region labeled by *CsChrimson.mVenus* differed from the peg MSN track (Fig. 4C, bottom). The SEZ regions containing bristle and peg MSN projections differed from those containing projections from *Gr5a*-, *Gr66a*-, *ppk28*-, and *E409*-expressing (*34*) GRNs (fig. S4A).

The differential axonal projections of peg and bristle MSNs in SEZ indicated that these neurons may play different roles in feeding. To examine the functions of bristle MSNs, we generated flies with *CsChrimson* expression exclusively in bristle MSNs by *FLP-FRT* recombination. We found that optogenetic activation of their bristle MSNs triggered a robust and reproducible spread of two labellar lobes (Fig. 4, D and E, and movie S6). Even after removal of the legs, wings, and antennae that also contain NOMPC-expressing MSNs, optogenetic activation of labella still triggered robust labellar spread (fig. S4B). However, it is difficult to rule out contributions of NOMPC-expressing MSNs in eye bristles or internal organs. In addition, the flies with *CsChrimson* expression in both bristle and peg MSNs also spread two labella upon optogenetic activation (Fig. 4E), which was still observed after blocking peg MSN synaptic transmission (Fig. 4F). These results demonstrated that bristle MSNs drive labellar spread.

Next, we examined the roles of peg MSNs in feeding. We found that optogenetic activation of flies with *CsChrimson* expression driven by *NP7506-Gal4* immediately retracted their proboscis during feeding (Fig. 4, G and H, and movie S7) but did not spread their labella (fig. S4C). In contrast, optogenetic activation of bristle MSNs did not induce proboscis retraction during feeding (fig. S4D). In addition to labeling peg MSNs, *NP7506-Gal4* also labels two to four bristle MSNs. To confirm that proboscis retraction was driven by peg MSNs, we screened more specific drivers and found that one *nompC-Gal4* (*30*) labeled ~10 peg MSNs but not any bristle MSN (fig. S4E and table S1). With this specific driver, we confirmed that optogenetic activation of peg MSNs induced proboscis retraction during feeding (Fig. 4H). Consistently, proboscis retraction was blocked by disruption of peg MSN synaptic transmission (Fig. 4I).

Neural circuits of mechanoreception-induced proboscis retraction

To map the circuits underlying proboscis retraction by peg MSNs, we examined *GMR58H01* neurons that were reported to label

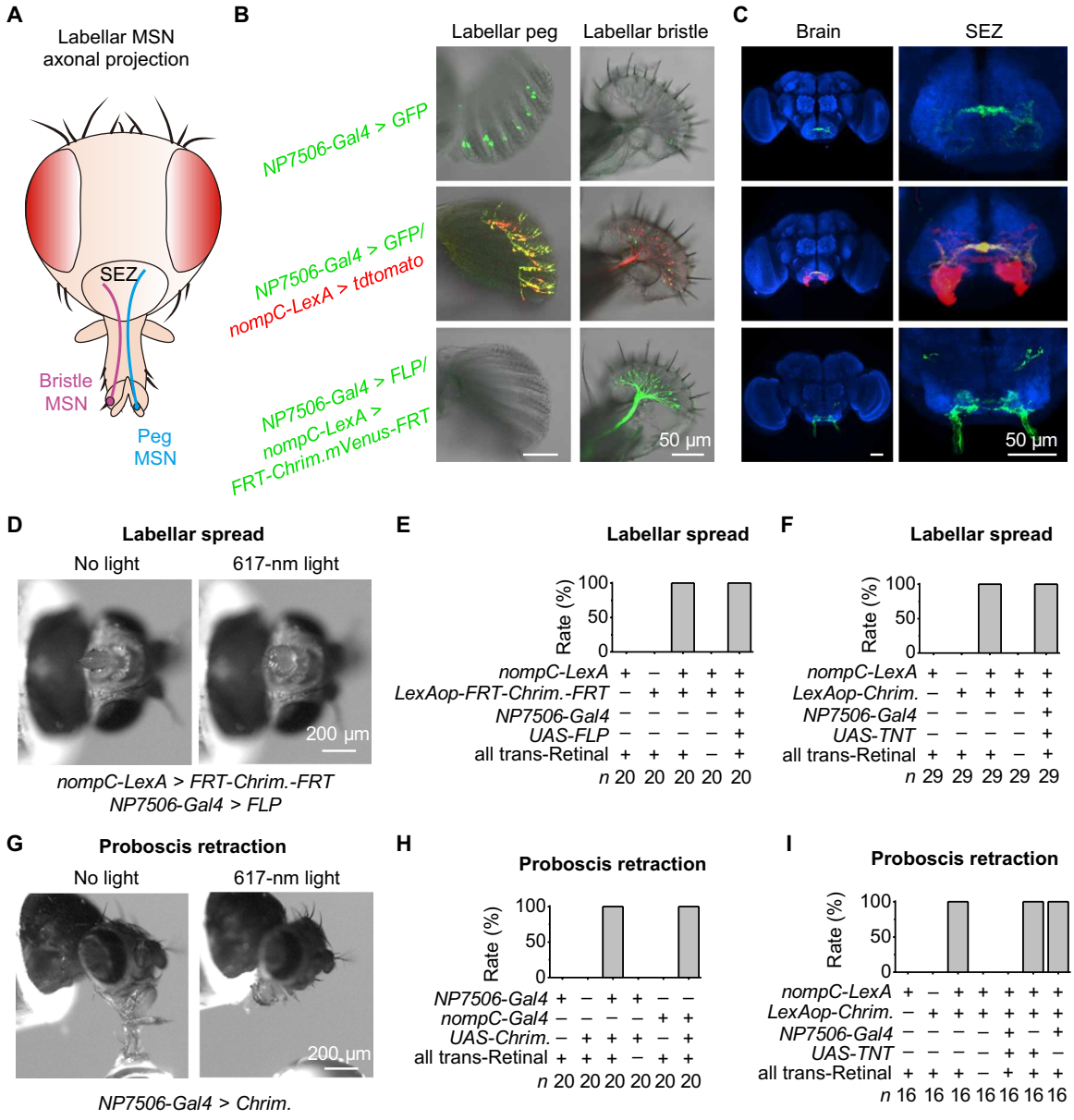

Fig. 4. Bristle MSNs and peg MSNs control distinct feeding behaviors. (**A**) Schematic illustration of axonal projections in SEZ by labellar MSNs. (**B**) Peg (left) and bristle (right) slices. *NP7506-Gal4* labels all peg MSNs and two to four bristle MSNs (top); *nompC-LexA* labels all peg MSNs and bristle MSNs (middle); *nompC-LexA*, *LexAop-FRT-CsChrimson.mVenus-FRT* together with *NP7506-Gal4/UAS-FLP* label exclusively bristle MSNs (bottom). (**C**) Distinct axonal projections of peg MSNs (top), peg and bristle MSNs (middle), and bristle MSNs (bottom). Red, tdtomato; green, GFP; blue, anti-nc82 immunostaining. (**D**) Bristle MSNs drive labellar spread. Optogenetic activation of bristle MSNs drives labellar spread. Light stimulation: 1 s, 617 nm. (**E**) Collective data of labellar spread by bristle MSNs. (**F**) Labellar spread does not require peg MSNs. (**G**) Peg MSNs drive proboscis retraction. Optogenetic activation of peg MSNs triggers proboscis retraction. Light stimulation: 1 s, 617 nm. (**H**) Collective data of proboscis retraction by peg MSNs. (**I**) Proboscis retraction requires peg MSNs.

motor neurons (MNs) for proboscis retraction (*35*). By expressing *CsChrimson* in *GMR58H01* neurons, we confirmed that their optogenetic activation induced proboscis retraction (fig. S5, A and B). Considering our observation that peg MSNs also drove proboscis retraction (Fig. 4G), we reasoned that *GMR58H01* neurons may receive sensory inputs from peg MSNs to drive proboscis retraction. To test this idea, we developed a labella-brain preparation that allowed us to perform patch-clamp recordings on these MNs. This preparation kept the labella intact and exposed the brain neurons to access by patch-clamp electrodes (Fig. 5A). There are four pairs of MNs labeled by *GMR58H01-Gal4* (*35*), which was confirmed by their expression of glutamate (Fig. 5B, left). Guided by their distinct brain positions, we performed patch-clamp recordings on these four pairs of MNs (Fig. 5B, middle). We found that only one pair of these MNs located at the anterior SEZ could be excited by peg MSNs (Fig. 5B, right), consistent with previous findings of their axonal projection to the muscles that control proboscis retraction (*35*).

The above results indicated that *GMR58H01* MNs are part of the circuit of proboscis retraction driven by peg MSNs. To examine the neural connections that link peg MSNs to *GMR58H01* MNs, we

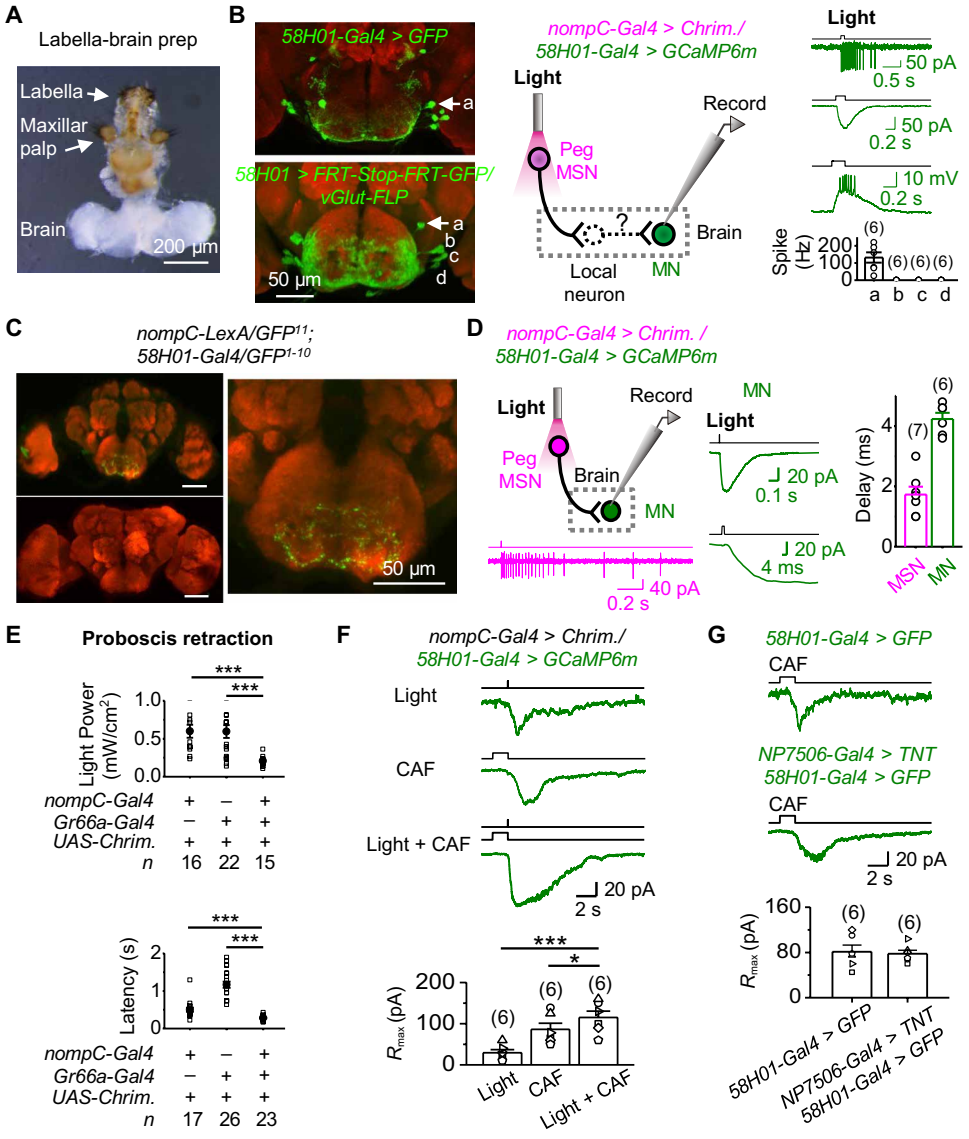

Fig. 5. Neural circuits of peg MSN–driven proboscis retraction. (**A**) A labella-brain preparation. (**B**) Patch-clamp recordings of *GMR58H01* MNs. Left: SEZ neurons labeled by *GMR58H01-Gal4* (top) and four pairs of SEZ MNs labeled by an intersection between *vGlut-FLP* and *GMR58H01-Gal4* (bottom). "a," "b," "c," and "d" mark the four pairs of MNs with similar positions as those MNs at the bottom. Middle: Illustration of simultaneous optogenetic activation of peg MSNs and patch-clamp recordings of *GMR58H01* MNs. Right: Electrical responses of *GMR58H01* MNs under cell-attached and perforated patch-clamp recordings and collective data. (**C**) GRASP between labellar MSNs and *GMR58H01* neurons. Left: GRASP signal between labellar MSNs and *GMR58H01* neurons (top); no GRASP signal in the absence of *GMR58H01* driver (bottom). Right: GRASP signal in SEZ (expanded from top left panel). (**D**) Monosynaptic transmission from peg MSNs to *GMR58H01* MNs. Left: Illustration of local optogenetic activation of labella and patch-clamp recordings on MNs in the brain (top) and spike firing in peg MSNs by optogenetic activation (bottom). Middle: Optogenetic activation of peg MSNs triggers an inward current in *GMR58H01* MNs (top) and at the expanded time scale (bottom). Right: Collective data of synaptic delay from peg MSNs to *GMR58H01* MNs. Light stimulation: 2 ms, 617 nm. (**E**) Bitter GRNs enhance peg MSN–driven proboscis retraction. Top: Proboscis retraction is more sensitive by coactivating peg MSNs and bitter GRNs. Light stimulation: 100 ms, 617 nm. Bottom: The latency of proboscis retraction is reduced by coactivation of peg MSNs and bitter GRNs. Light stimulation: 617 nm, 1.75 mW/cm^2, 1 s. ***$P < 0.001$. (**F**) Inward currents of *GMR58H01* MNs triggered by peg MSNs and bitter GRNs. Top: Current of *GMR58H01* MNs driven by optogenetic activation of peg MSNs, bitter GRNs, and peg MSNs and bitter GRNs together. Bottom: Collective data. CAF, 20 mM. Light stimulation: 617 nm, 1.75 mW/cm^2. *$P < 0.05$ and ***$P < 0.001$. (**G**) Activation of *GMR58H01* MNs by bitter GRNs independently of peg MSNs. Inward currents of *GMR58H01* MNs driven by bitter GRNs (top) is intact when synaptic transmission of peg MSNs is blocked (middle); collective data (bottom). CAF, 20 mM.

performed synaptic labeling with GFP reconstitution across synaptic partners (GRASP) (*13*, *36*). We found strong GRASP signals in the SEZ between the neurons labeled by *nompC-LexA* and *GMR58H01-Gal4* (Fig. 5C), suggesting that these neurons might be in close contact. However, the peg MSN driver (*nompC-LexA*) also labels other MSNs, and the proboscis retraction MN driver (*GMR58H01-Gal4*) labels some other MNs; thus, the GRASP signals may not be specific to the contact between peg MSNs and *GMR58H01* MNs. Next, we examined whether peg MSNs and *GMR58H01* MNs form direct synaptic connections by combining patch-clamp recordings and an optogenetic approach. We found that the synaptic delay in *GMR58H01* MNs triggered by local optogenetic activation of peg MSNs was approximately 2 ms (Fig. 5D),

strongly indicating a direct, monosynaptic transmission from peg MSNs to *GMR58H01* MNs (*37*). One caveat of these experiments is that *GMR58H01* MNs also expressed CsChrimson, and stray light may activate the MNs directly. Nonetheless, the monosynaptic connections were further supported by the elimination of *GMR58H01* MN responses by synaptic transmission blockage by tetrodoxin (TTX) (fig. S5C) and a lack of *GMR58H01* MN responses to local labellar light stimulations in the absence of *nompC-Gal4* driver (fig. S5D).

Bitter taste is known to inhibit feeding. Consistently, we found that optogenetic activation of *Gr66a*-expressing GRNs also induced proboscis retraction (fig. S5E). When peg MSNs and bitter GRNs were coactivated, proboscis retraction was more sensitive to optogenetic activation (Fig. 5E, top), and the retraction speed was faster than that driven by each single group of neurons (Fig. 5E, bottom). To investigate the underlying neural mechanisms, we performed patch-clamp recordings on *GMR58H01* MNs and found that they could also be excited by bitter GRNs (Fig. 5F). Bitter GRN–induced excitatory responses were additive to peg MSN–induced responses (Fig. 5F), consistent with their synergistic behavior interactions (Fig. 5E). When the synaptic transmission of peg MSNs was blocked, bitter GRN–induced responses in *GMR58H01* MNs were intact (Fig. 5G), suggesting that activation of *GMR58H01* MNs by bitter GRNs was not through a direct activation of peg MSNs.

Neural circuits of mechanoreception-induced labellar spread

To dissect the neural circuit of labellar spread by bristle MSNs, we examined *GMR18B07* neurons that were reported to control labellar spread (*35*). Using optogenetic tools, we confirmed that *GMR18B07* neurons could drive labellar spread (fig. S6A). *GMR18B07-Gal4* was reported to label four pairs of MNs (*35*), which were confirmed by their glutamate expression (Fig. 6A, left). Considering our observation that bristle MSNs also drive labellar spread, we speculated that *GMR18B07* MNs receive sensory inputs from bristle MSNs to drive labellar spread.

To test the above hypothesis, we performed patch-clamp recordings on *GMR18B07* MNs to examine their synaptic inputs (Fig. 6A, middle). Among these MNs, we found that only one pair of MNs located at the dorsal SEZ region was excited by bristle MSNs (Fig. 6A, right), which were likely the MNs that control labellar spread (*14*). Furthermore, we found GRASP signals between labellar MSNs and *GMR18B07* neurons (Fig. 6B), suggesting a possible contact, which is, however, confounded by nonspecific drivers. Next, by combining optogenetics and patch-clamp recordings, we investigated the functional connections between bristle MSNs and *GMR18B07* neurons. The synaptic delay in *GMR18B07* MNs induced by activation of bristle MSNs was short at ~2 ms (Fig. 6C), strongly suggesting that bristle MSNs and *GMR18B07* MNs form direct, monosynaptic connections. This conclusion is further supported by the elimination of *GMR18B07* MN responses by TTX (fig. S6B).

Bitter application to the labella completely blocked labellar spread induced by bristle MSNs (Fig. 6D). Similarly, coactivation of bitter GRNs optogenetically also blocked labellar spread by bristle MSNs (fig. S6C). To investigate the neural mechanisms underlying such a cross-modality inhibition, we performed patch-clamp recordings of *GMR18B07* MNs and found that bitter GRNs inhibited bristle MSN–induced excitatory responses (Fig. 6E, top). However, bitter GRNs alone did not produce any excitatory or inhibitory responses (fig. S6D). Similarly, we found that γ-aminobutyric acid (GABA)

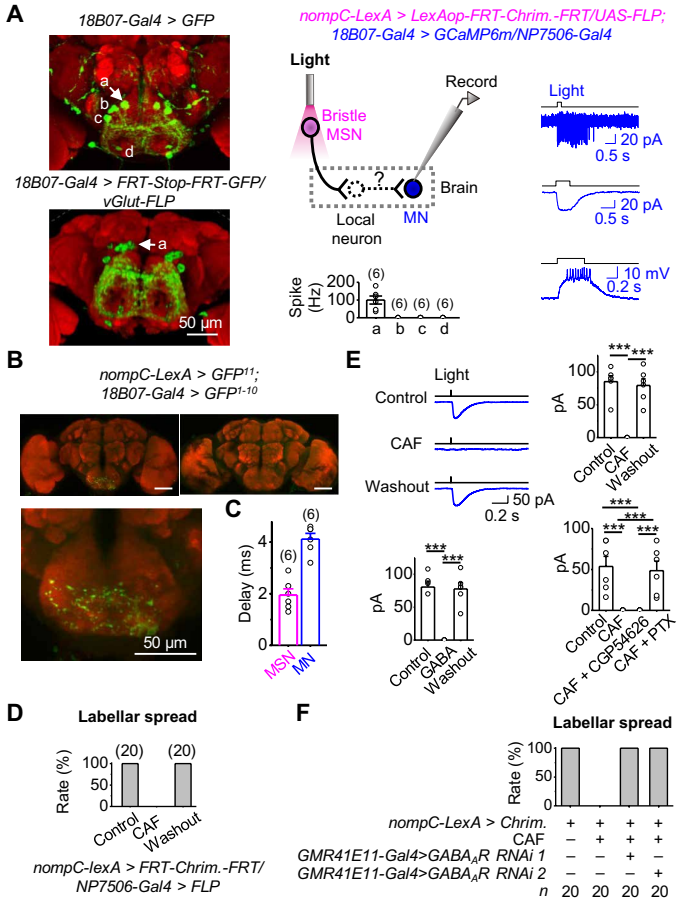

Fig. 6. Neural circuits of bristle MSN–driven labellar spread. (**A**) Patch-clamp recordings of *GMR18B07* MNs. Left: SEZ neurons labeled by *GMR18B07-Gal4* (top) and four pairs of SEZ MNs labeled by intersection with *vGlut-FLP* and *GMR18B07-Gal4* (bottom). a, b, c, and d mark the four pairs of MNs. Middle: Illustration of simultaneous optogenetic activation and patch-clamp recordings (top); collective data (bottom). Right: Electrical responses of *GMR18B07* MNs under cell-attached recordings (top), voltage-clamped in perforated patch-clamp recordings (middle), and current-clamped in perforated patch-clamp recordings (bottom). (**B**) GRASP between labellar MSNs and *GMR18B07* neurons. Top: GRASP signal between labellar MSNs and *GMR18B07* neurons (left); no GRASP signal in the absence of *GMR18B07* driver (right). Bottom: GRASP signal in the SEZ (expanded from top left panel). (**C**) Monosynaptic connections between bristle MSNs and *GMR18B07* MNs. Collective data of synaptic delay from bristle MSNs to *GMR18B07* MNs ($n = 6$). Light stimulation: 2 ms, 617 nm. (**D**) Bitter GRNs inhibit bristle MSN–driven labellar spread. CAF, 50 mM. (**E**) Bitter GRNs inhibit bristle MSN–driven responses of *GMR18B07* MNs. Top: Bristle MSN–driven responses of *GMR18B07* MNs in Ringer, CAF, and after wash out CAF (left) and collective data (right). Bottom: Collective data of γ-aminobutyric acid (GABA) blockage of bristle MSN–driven responses of *GMR18B07* MNs (left); $GABA_A$ receptor antagonist blocks inhibition of bristle MSN–driven responses of *GMR18B07* MNs by bitter GRNs (right). CAF, 20 mM; GABA, 1 mM; CGP54626, 25 μM; PTX, 25 μM. ***$P < 0.001$. $n = 6$. (**F**) Knocking down $GABA_A$ receptor eliminates inhibition of bristle MSN–driven labellar spread by bitter GRNs.

completely blocked the bristle MSN–induced responses in *GMR18B07* MNs (Fig. 6E, bottom left). The blockage of bristle MSN–driven responses by bitter GRNs was eliminated by picrotoxin [a GABA type A ($GABA_A$) receptor antagonist] but not by CGP54626 (a $GABA_B$ receptor antagonist) (Fig. 6E, bottom right). Together, these results suggested that bitter GRNs may inhibit synaptic transmission from

bristle MSNs to *GMR18B07* MNs through $GABA_A$ receptor activation. Bitter GRNs likely recruit some GABAergic (GABA-releasing) interneurons because there was no GRASP signal between bitter GRNs and labellar MSNs (fig. S6E).

To further test the above possibility, we performed behavioral assays of labellar spread by knocking down the $GABA_A$ receptors of labellar MSNs with RNA interference (RNAi). Using two independent RNAi lines, we found that labellar MSN $GABA_A$ receptor knockdown removed the blockage of bristle MSN–driven labellar spread by bitter stimulations (Fig. 6F).

DISCUSSION

Among the various sensory modalities, mechanoreception is the least well understood. Mouth mechanoreception detects the physical properties of food (*6*–*8*), but the central circuits mediating its feeding control are unknown. In addition, whether and how mouth mechanoreception integrates with gustation to shape feeding decision remain largely unknown. Here, we found that mouth mechanoreception can facilitate and terminate *Drosophila* feeding through two distinct central motor circuits. Furthermore, these two mechanosensory circuits integrate with bitter taste in opposing manners to shape feeding behaviors.

Several mechanosensitive channels have been identified in *Drosophila* (*8*, *22*–*29*). However, how these channels mediate mechanosensory signaling in native adult *Drosophila* MSNs remains unclear. In the auditory system of *Drosophila*, multiple lines of evidence (*31*, *38*, *39*) suggest that NOMPC mediates mechanotransduction in Johnston's organ neurons (JONs) and that NANCHUNG and INACTIVE amplify the NOMPC-transduced signals. However, a recent study challenged this view by proposing that NANCHUNG and INACTIVE are mechanotransduction channels and that NOMPC plays an amplification role in JONs (*32*).

Similarly, the roles of these TRPs in bristle MSNs also remain unclear. The loss of NOMPC reportedly decreases the mechanically induced responses in fly notum bristles (*28*). However, the residual mechanical responses of field potentials remaining in $nompC^3$ notum bristles imply the existence of other non-NOMPC channels. In recurved bristles of the wings, NANCHUNG but not NOMPC has been reported to mediate mechanotransduction (*40*). However, both NANCHUNG (*6*) and NOMPC (*7*) have been shown to mediate mechanoreception by labellar bristles. Resolving the specific roles of these TRPs in mechanosensory signaling would be facilitated by obtaining patch-clamp recordings from the native *Drosophila* MSNs, a long-standing challenge in the field (*32*).

We developed a labellar slice preparation enabling the first patch-clamp recordings of mechanotransduction receptor currents in native *Drosophila* labellar MSNs. In this preparation, all accessory structures involved in relaying force stimuli to mechanosensitive channels remained intact, thereby allowing the investigation of mechanosensory responses to physiological stimuli. By mechanically deflecting the sensillum, we examined the MSNs of both taste pegs and bristles. The latency of their mechanotransduction currents was approximately 3 ms, consistent with the response kinetics of the field potential recorded in fly notum bristles (*28*). The fast response kinetics suggests that the transduction channels in native *Drosophila* MSNs are directly gated by force. Furthermore, we found that the I-V relationship of the mechanotransduction currents was linear and reversed at ~ 7 mV, suggesting that nonselective transduction cation channels are present in native MSNs. Both the action potential firing and mechanotransduction receptor currents were intact in nan^{36a} and iav^1 flies but completely eliminated in $nompC^3$ flies. Rescuing NOMPC expression in labellar MSNs restored the mechanotransduction currents in $nompC^3$ flies. Together, these data strongly suggested that both peg and bristle MSNs used NOMPC but not NANCHUNG/INACTIVE for mechanotransduction, consistent with previous findings (*7*, *25*, *28*).

During feeding, bristle and peg MSNs are sequentially stimulated and thus can convey different features about the food. Taste bristles are located on the outer labellar surface and are stimulated by food contact before the opening of the labellar lobes, thus providing information about the availability and location of food. In contrast, taste pegs reside in the inner labellar surface, and their MSNs are activated by food contact only after labellar spread. The pegs are short and covered by cuticle folds (Fig. 3A); thus, peg MSNS require stronger mechanical stimuli for activation than bristle MSNs (Figs. 2E and 3E). Therefore, peg MSNs may report food quality, such as food hardness, to evaluate whether the food is indeed ingestible. Consistently, we found that the MSNs in taste bristles and pegs directed two distinct feeding behaviors. Activation of bristle MSNs drove labellar spread, thus acting as a feeding gate for food exposure to the inner labellar surface. In contrast, activation of peg MSNs triggered proboscis retraction, thus protecting the fly from the intake of noningestible foods. The idea that bristle MSNs report food availability and that peg MSNs evaluate food ingestibility is further supported by the results of a natural feeding test. In starved flies, labellar spread occurred immediately upon food contact regardless of food hardness; however, the time spent on food exploration and ingestion after labellar spread was dependent on food hardness (fig. S6F).

Both of these feeding behaviors are reflex responses because the bristle and peg MSNs make direct, monosynaptic connections with distinct MNs in the brain. The anatomical and functional differences between mechanosensory circuits of bristle and peg MSNs reveal that mechanoreception by the labella is processed through a labeled-line strategy, enabling the fly to control two distinct feeding behaviors by using a single type of mechanosensitive channel. This strategy may also be used by mammalian touch sense, in which similar mechanosensitive channels but distinct cellular context and neural circuits may be used to generate rich sensations from a gentle breeze to a harsh pinch.

The fly labella receive a multitude of sensory inputs, such as gustatory and mechanical cues. This modality-specific sensory information must be integrated in the brain to produce a coherent feeding output. However, the mechanism by which these sensory inputs are integrated to coordinate feeding remains poorly understood. Here, we showed that the bitter sense oppositely regulated two mechanoreception-driven feeding circuits and behaviors. The labellar spread driven by bristle MSNs was inhibited by bitter-sensing GRNs. In contrast, bitter sense promoted proboscis retraction driven by peg MSNs. Therefore, bitter sense acts as a powerful gate control for labellar spread but a co-driver for proboscis retraction, both of which enable the fly to avoid the intake of toxic foods.

In summary, our work reveals how mouth mechanoreception directs *Drosophila* feeding. Although both peg and bristle MSNs rely on the same NOMPC to detect mechanical force through food contact, they provide distinct food information. By monosynaptic connections with different MNs in the brain, these MSNs drive two feeding actions in a reflex manner. During feeding, these reflex responses are subject to opposite regulation by bitter sensation. Given that

mammalian mouthparts also harbor many MSNs, we anticipate that our work might help to unravel the roles of mechanoreception in mammalian feeding.

MATERIALS AND METHODS

Fly stocks

All flies were raised on standard cornmeal agar medium, under 60% humidity and a 12-hour-light/12-hour-dark cycle at 25°C. *Gr5a-LexA*(VP16) (*13*) and *E409-Gal4* (*34*) were from K. Scott. *Gr5a-Gal4* (II) and *Gr66a-Gal4* (III) were from J. Carlson. *ppk28-Gal4*, $ppk28^{\Delta}$ (*23*, *29*), and $ppk26^{Gal4}$ (*27*) were from Z. Wang. $nompC^{3}$ (*25*, *31*) and *nompC-Gal4* (III) (*30*) were from X. Liang. *Gr66a-Gal4* (II) and tmc^{1} (*8*) were from C. Montell. $Pain^{3}$ (*26*), *LexAop-mCD4::spGFP*^{11};*UAS-mCD4::spGFP*$^{1\text{-}10}$, *20XUAS-IVS-SYN21-GFP-P10*, and *VGlut-flp* were from Y. Rao. *UAS-RDL-RNAi* was from Y. Li. *UAS>stop>myrGFP* was from C. Zhou. *UAS-FLP* (II) was from Y. Pan. *UAS-FLP* (III) and *UAS-mCD8-GFP* were from C. Potter. The following stocks were obtained from Bloomington Drosophila Stock Center (BDSC): *nompC-QF* (BDSC nos. 36346 and 36349), *nompC-LexA* (BDSC nos. 52240 and 52241), *nompC-Gal4* (BDSC nos. 36361 and 36369), *NP7506-Gal4* (BDSC no. 114319), *GMR41E11-Gal4* (BDSC no. 50131), *GMR57C10-Gal4* (BDSC no. 39171), *GMR18B07-Gal4* (BDSC no. 47476), *GMR58H01-Gal4* (BDSC no. 39197), *GAD1-Gal4* (BDSC no. 51630), *UAS-GCaMP6m* (BDSC no. 42750), *UAS-CsChrimson* (BDSC nos. 55135 and 55136), *UAS-TNT* (BDSC no. 28837), *LexAop-GFP* (BDSC no. 32209), *LexAop-CsChrimson* (BDSC nos. 55138 and 55139), *LexAop-tdtomato* (BDSC no. 56142), *QUAS-mtdtomato* (BDSC no. 30005), *QUAS-GFP* (BDSC no. 30002), nan^{36a} (BDSC no. 24902), iav^{1} (BDSC no. 101174), $piezo^{KO}$ (BDSC no. 58770), and *UAS-nSyb-spGFP*$^{1\text{-}10}$,*LexAop-CD4-spGFP*^{11} (BDSC no. 64314). The following stock was obtained from Vienna *Drosophila* Resource Center (VDRC): *DmRdl-RNAi* (VDRC no. 41103). All experimental genotypes used in this study are listed in table S2.

Generation of transgenic flies

To generate *LexAop-nompC-L-GFP-2A-tdtomato* flies, we subcloned *nompC-L His-GFP* from pOCC8 nompC-L His-GFP [the plasmid was a gift from Z. Wang (Institute of Neuroscience, China)] using the following primer sequences: 5′-cctttacttcaggcggccgcggcccgcaatgtcgcagccgcgcg-3′ (forward) and 5′-gttggtggcggtaccgctgcctccactgtgatggtgatggtg-3′ (reverse). *tdtomato* was subcloned from pDEST-HemmarR tdtomato [the plasmid was a gift from Y. Rao (Peking University, China)] using the following primer sequences: 5′-ggcagcggtaccgccaccaacttcagcctgctgaagcaggccggcgatgtggaggagaaccccgggcccatggtgagcaagggcgaggag-3′ (forward) and 5′-gtaaggttccttcacaaagatcctttagagggcaacttcattttc-3′ (reverse). We inserted *nompC-L His-GFP* and *tdtomato* into pJFRC19-13XLexAop2-IVS-myrGFP vector and then injected the LexAop-nompC-L-GFP-2A-tdtomato plasmids into the transgenic flies (BDSC no. 25710).

To generate *LexAop2-FRT-CsChrimson.mVenus-FRT* flies, we subcloned *CsChrimson.mVenus* from the fly *20XUAS-IVS-CsChrimson.mVenus* (BDSC no. 55135) using the following primer sequences [containing the FRT (flipase recognition target) sequence]: 5′-cttatcctttacttcaggcggccgcgaagttcctatactttctagagaataggaacttcgccaccatgagcagactggtcgccgctt-3′ (forward) and 5′-aggttccttcacaaagatcctctagagaagttcctattctctagaaagtataggaacttcttacacctcgttctcgtagcaga-3′ (reverse).

CsChrimson.mVenus was inserted into the *Not I*/*Xba I*–digested pJFRC19-13XLexAop2-IVS-myrGFP vector (Addgene no. 26224), and the LexAop2-FRT-CsChrimson.mVenus-FRT plasmids were injected into the transgenic flies (BDSC no. 25710).

Electrophysiological recordings

Labellar slices

Young adult flies (1 to 4 days after eclosion) were immobilized on ice. The labella were isolated, and each labellar lobe was cut into transverse slices in *Drosophila* saline. To record bristle MSNs, the cut was made parallel and close to the inner labellar surface; to record peg MSNs, the cut was also made parallel to the inner labellar surface, and the inner labellar part was kept intact. The labellar slice was stabilized in the recording chamber and continuously perfused with 95% O_2/5% CO_2 (v/v)–bubbled *Drosophila* saline. The saline contained the following: 178 mM NaCl, 3 mM KCl, 4 mM $MgCl_2$, 1.5 mM $CaCl_2$, 26 mM $NaHCO_3$, 1 mM NaH_2PO_4, 5 mM *N*-tris(hydroxymethyl) methyl-2-aminoethanesulfonic acid (TES), and 5 mM trehalose, bubbled with 95% O_2/5% CO_2 (pH 7.4). The dissection solution was made by replacing $NaHCO_3$, NaH_2PO_4, and TES in *Drosophila* saline with 5 mM Hepes and 27 mM NaCl (pH 7.4, adjusted with NaOH), bubbled with oxygen. All chemicals were obtained from Sigma-Aldrich and were freshly dissolved in *Drosophila* saline daily.

Neurons were visualized on an upright microscope (Scientifica) with infrared (IR)–differential interference contrast (Olympus). The image was captured with an IR charge coupled device (DAGE-MTI) and displayed on a television monitor (Sony).

Patch-clamp recordings were made with MultiClamp 700B (Molecular Devices). The patch electrodes were made from borosilicate glass (WPI) with a P-1000 or P-97 puller (Sutter). The cell bodies of sensory neurons in labellar slices were small (diameter, 3 to 4 μm), thus requiring a recording pipette tip of ~ 0.2 μm and a resistance of ~15 to 20 megohms filled with intracellular saline [185 mM K-gluconate, 5 mM NaCl, 2 mM $MgCl_2$, 0.1 mM $CaCl_2$, 1 mM EGTA, and 10 mM Hepes (pH 7.4); ~390 mOsm]. For perforated patch-clamp recordings, amphotericin B was dissolved in dimethyl sulfoxide, diluted with intracellular saline to a final concentration of 200 μg/ml, and backfilled into the recording pipette. For whole-cell patch-clamp recordings, guanosine 5′-triphosphate (GTP)–tris (0.5 mM) and Mg–adenosine 5′-triphosphate (ATP) (4 mM) were added to the intracellular saline. For suction-pipette recordings, a recording pipette with a tip diameter of ~ 2 μm and a resistance of ~2 megohms filled with dissection solution was used. Typically, a loose seal (~15 megohms) between the recording pipette and cell body was obtained. To access the cell bodies of MSNs, a suction-recording pipette filled with protease XIV (2 mg/ml; Sigma) was used to locally digest the sheath cells that wrap a neural cluster of either a peg or bristle.

To measure the I-V relationship, voltage-sensitive Na^+ channels and K^+ channels were blocked by a mixture of TTX (50 nM), tetraethylammonium chloride (10 mM), and sometimes also 4-AP (10 mM). Current and voltage signals were digitized and recorded with Digidata 1440A and pClamp 10.2 (Molecular Devices), filtered at 2 kHz, and sampled at 5 kHz. Recorded currents were low-pass–filtered at 200 Hz (unless stated otherwise) for display. The voltage was clamped at −80 mV unless stated otherwise. Measured voltages were corrected for a liquid junction potential.

Labella-brain preparation

Young adult flies (1 to 4 days after eclosion) were immobilized on ice. The head was dissected and transferred to a recording chamber. The antenna, compound eyes, and brain cuticle were removed by

fine forceps. The labella-brain preparation was then stabilized in the chamber with the anterior side up, continuously perfused with a saline solution bubbled with 95% O_2/5% CO_2 (pH 7.4) at room temperature. The saline was composed of the following: 103 mM NaCl, 3 mM KCl, 4 mM $MgCl_2$, 1.5 mM $CaCl_2$, 26 mM $NaHCO_3$, 1 mM NaH_2PO_4, 5 mM TES, 20 mM D-glucose, 17 mM sucrose, and 5 mM trehalose. For whole-cell patch-clamp recordings, the recording pipette was filled with internal solution consisting of the following: 140 mM K-gluconate, 6 mM NaCl, 2 mM $MgCl_2$, 0.1 mM $CaCl_2$, 1 mM EGTA, and 10 mM Hepes (pH 7.2), with an osmolarity of 270 mOsm. For perforated patch-clamp recordings, the pipette was backfilled with the internal solution that contains amphotericin B (200 μg/ml) and then filled with regular internal solution. For cell-attached recordings, the pipette was filled with the saline solution with $NaHCO_3$ replaced by 10 mM Hepes (pH 7.2).

Mechanical and chemical stimulation

Sensillar deflection was achieved by pushing the sensillar bristle with a glass pipette, which was similar to the suction-recording pipette and has a "7-shaped" tip. The pipette was attached to a piezo actuator (Physik Instrumente), which was mounted on a micromanipulator (Scientifica). Mechanical deflection was quantified by the movement of the glass pipette. Under the 60× water lens, the pipette tip was positioned against the mid-point of a targeted sensillar bristle. The piezo actuator was controlled by voltage signals from the analog output of Digidata 1440 (Molecular Devices).

For chemical stimulation of the sensory neurons in the labellar slice, rapid solution changes were used. The rapid solution change was produced by translating the interface between the two following streams across the recorded labellar sensory neurons with an electronic stepper (Warner Instruments). Different solutions ran through a three-barrel tube (Warner Instruments), whose tips were positioned ~100 μm away from the labellar slice. The solution flow was driven by gravity and was controlled by solenoid valves (The Lee Company) and a valve controller (AutoMates Scientific). The inner width of each square barrel of the perfusion tubing was ~600 μm, emitting a solution readily covering the labellar slice.

Optogenetic stimulation in electrophysiological recordings

Flies expressing *CsChrimson* were raised on standard food. Labellar slices or labella-brain preparations were first incubated in the Hepes-buffered saline with 100 μM all trans-Retinal (Sigma-Aldrich) for 20 to 25 min and then washed and perfused with regular saline bubbled with 95% O_2/5% CO_2 (pH 7.4). The labella were stimulated with a red light-emitting diode (617 nm; M617F1, Thorlabs) of 1.75 mW/cm^2 through an optic fiber (inner diameter, 200 μm) that was positioned approximately 50 μm away. Light intensity was measured by a power meter (Model 1936-R, 918D-ST-UV, Newport).

Single-cell labeling by neurobiotin

Neurobiotin (Vector Lab) was dissolved in a modified internal solution [70 mM K-gluconate, 6 mM NaCl, 2 mM $MgCl_2$, 0.1 mM $CaCl_2$, 1 mM EGTA, 4 mM Mg-ATP, 0.5 mM GTP-tris, and 10 mM Hepes (pH 7.4)] for osmolarity balance of the 2% neurobiotin. The recording pipette was filled with neurobiotin-containing internal solution. After breaking into whole-cell mode, depolarizing currents (200 ms, 2 Hz) were injected for 20 min, which facilitated diffusion of positively charged neurobiotin into the recorded neuron. The recording pipette was gently detached from the cell after another 20-min wait of neurobiotin diffusion within the cell. The labellar preparation was transferred into 4% paraformaldehyde, fixed for 4 hours on ice, and then washed by phosphate-buffered saline (PBS) for three times at a 20-min interval, blocked in 5% bovine serum albumin in PBST (1% Triton X-100 in PBS) for 2 hours at room temperature. The preparations were incubated with Streptavidin-568 (1:500; Invitrogen, catalog number S11226) overnight at 4°C, washed by PBST (1% Triton X-100 in PBS) for three times at an interval of 20 min, and then mounted in the glycerol. Images were acquired on a Nikon A1R+ confocal microscope with a 25× water immersion objective.

Synaptic labeling by GRASP and immunostaining

The fly brains were dissected in PBS, transferred to 4% paraformaldehyde (on ice) for 1 hour, and then washed by PBS and blocked in 5% normal goat serum (1% Triton in PBS) for 2 hours at 23°C. After incubation with mouse anti-nc82 [1:100; DSHB (Developmental Studies Hybridoma Bank) catalog number nc82] overnight at 4°C, the brains were washed three times with 0.5% PBST, followed by incubation of secondary antibodies, Alexa Fluor 568–congugated anti-mouse and Alexa Fluor 647–conjugated anti-mouse (1:200 each; Invitrogen, catalog numbers, A-11004 and A-32728, respectively), for 6 hours at room temperature. The brains were washed three times and then mounted in glycerol. Images were acquired in 0.5-μm sections on a Nikon A1R+ confocal microscope with a 25× water immersion objective.

Behavioral assays

Flies (2 to 3 days after eclosion) were food-deprived on a wet Kimwipe for 24 hours. The fly was anesthetized on ice and inserted into a 1-ml pipette tip with the fly head and proboscis exposed. To conduct proboscis extension reflex and labellar spreading experiments, a 1-ml syringe was used to apply a small drop of sucrose solution (500 mM) to the labella or forelegs. To conduct proboscis retraction experiments, a small drop of sucrose solution (500 mM) was used to stimulate the labella and engage the fly to feeding. The behaviors were recorded under a dissection microscope (M205, Leica) with a color camera (DFC450 C, Leica).

For optogenetic behavioral experiments, flies were raised on standard food mixed with 100 μM all trans-Retinal. Newly enclosed flies were collected and starved for 24 hours. The fly proboscis was stimulated with red light (617 nm; M617F1, Thorlabs). The light intensity is of 1.75 mW/cm^2 unless stated otherwise.

For natural feeding experiments, a drop of food was placed in a small cavity of a sylgard-coated plate and covered by a coverslip, thus facilitating the video capture by limiting the range of fly walking. When food was omitted, this setup could be also used to provide physical touch of the coverslips for the extended proboscis induced by optogenetical activation of sweet-sensing GRNs. The behaviors were recorded with a high-speed camera (MV-A5031MU815, Dahua Technology).

Scanning electron microscopy

Samples were collected and fixed in 0.1 M phosphate buffer (pH 7.4) that contains freshly prepared 2.5% glutaraldehyde for 4 hours at room temperature. Samples were washed by 0.1 M phosphate buffer three times at a 10-min interval and then post-fixed in 1% OsO_4 for 1 hour at room temperature. Subsequently, the samples were washed with 0.1 M phosphate buffer three times and then treated with increasing concentrations of acetone (30, 50, 70, 85, 90, 95, and 100%) for approximately 10 min in each solution, followed by three washes in 0.1 M phosphate buffer. Samples were treated with critical point drying, mounted on a scanning electron microscope (SEM) stub with a copper tap, and then sputter-coated with gold for 1.5 min. Images were collected with a scanning electron microscope (FEG QUANTA 450) at 20 kV.

Focused ion beam SEM

Samples were collected and fixed in 0.1 M phosphate buffer (pH 7.4), containing freshly prepared 4% (w/v) paraformaldehyde and 2.5% glutaraldehyde for 2 hours at room temperature and then overnight at 4°C. Specimens were washed and post-fixed in 1% OsO_4 with 2% potassium ferrocyanide for 1 hour at room temperature. After rinsing several times in phosphate buffer, samples were dehydrated in a graded ethanol series and embedded in Spurr's resin (SPI Supplies, PA, USA). Focused ion beam SEM imaging was performed with a Helios Nanolab G3 UC scanning electron microscope (Thermo Fisher Scientific), and the automated data collection was guided by the Auto Slice and View G3 1.7.2 software (Thermo Fisher Scientific). The samples were imaged in the backscattered electron mode with through-the-lens and in-column detectors. The ion beam milling was performed at 30 kV and 2.5 nA, and images were recorded with an electron beam at 2 kV and 0.2 nA and a working distance of 2 mm. The image resolution was 6144 × 4096 with a horizontal filed width of 16.8 μm, and the *z*-step size was 20 nm.

Quantification of the time of proboscis retraction

We used two independent analysis methods to quantify the time of proboscis retraction. One is to manually count the video frames one by one; the other is computer-assisted image processing. For manual analysis, the frames were counted from the frame with the start of optogenetic activation until the video frame with a full proboscis retraction. For computer-aided analysis, the image processing software was written in MATLAB. In the videos, the experimental fly appears bright in a black ground under IR illumination. The fly was stabilized in a pipette tube, which only allows the proboscis to move. Thus, the change of brightness area in the video frames reflects the movement of proboscis. The maximal reduction in the brightness area indicates a final proboscis retraction. The time of proboscis retraction is calculated as the total frames from optogenetic activation to a full proboscis retraction time the duration a single frame. These two methods yield similar results.

Statistics

Data are presented as mean values accompanied by SEM. Statistical parameters including the exact value of *n*, precision measures (means ± SEM), and statistical significance were reported in the figure legends.

SUPPLEMENTARY MATERIALS

Supplementary material for this article is available at http://advances.sciencemag.org/cgi/content/full/5/5/eaaw5141/DC1

Fig. S1. Labellar spread.
Fig. S2. Mechanosensitivity in varied bristles and dendritic pattern of bitter GRNs.
Fig. S3. Mechanosensitivity of *GMR41E11*-labeled bristle neurons.
Fig. S4. Axonal projections and functions of labellar MSNs.
Fig. S5. *GMR58H01* neurons and bitter GRNs drive proboscis retraction.
Fig. S6. *GMR18B07* neurons drive labellar spread.
Table S1. Expression patterns of different driver lines.
Table S2. Full experimental genotypes.
Movie S1. Labellar spread during natural feeding.
Movie S2. Labellar spread by food contact of labella.
Movie S3. Sweet GRNs do not drive labellar spread.
Movie S4. Mechanical stimulation induces labellar spread.
Movie S5. Three-dimensional reconstruction of a taste bristle.
Movie S6. Labellar spread by bristle MSNs.
Movie S7. Proboscis retraction by peg MSNs.

REFERENCES AND NOTES

1. L. B. Vosshall, R. F. Stocker, Molecular architecture of smell and taste in *Drosophila*. *Annu. Rev. Neurosci.* **30**, 505–533 (2007).
2. H. Amrein, N. Thorne, Gustatory perception and behavior in *Drosophila melanogaster*. *Curr. Biol.* **15**, R673–R684 (2005).
3. R. M. Joseph, J. R. Carlson, *Drosophila* chemoreceptors: A molecular interface between the chemical world and the brain. *Trends Genet.* **31**, 683–695 (2015).
4. D. A. Yarmolinsky, C. S. Zuker, N. J. P. Ryba, Common sense about taste: From mammals to insects. *Cell* **139**, 234–244 (2009).
5. Z. Wang, A. Singhvi, P. Kong, K. Scott, Taste representations in the *Drosophila* brain. *Cell* **117**, 981–991 (2004).
6. Y. T. Jeong, S. M. Oh, J. Shim, J. T. Seo, J. Y. Kwon, S. J. Moon, Mechanosensory neurons control sweet sensing in *Drosophila*. *Nat. Commun.* **7**, 12872 (2016).
7. J. A. Sánchez-Alcañiz, G. Zappia, F. Marion-Poll, R. Benton, A mechanosensory receptor required for food texture detection in *Drosophila*. *Nat. Commun.* **8**, 14192 (2017).
8. Y. V. Zhang, T. J. Aikin, Z. Li, C. Montell, The basis of food texture sensation in *Drosophila*. *Neuron* **91**, 863–877 (2016).
9. M. Trulsson, R. S. Johansson, Orofacial mechanoreceptors in humans: Encoding characteristics and responses during natural orofacial behaviors. *Behav. Brain Res.* **135**, 27–33 (2002).
10. V. G. Dethier, *The Hungry Fly* (Harvard Univ. Press, 1976).
11. T. F. Flood, S. Iguchi, M. Gorczyca, B. White, K. Ito, M. Yoshihara, A single pair of interneurons commands the *Drosophila* feeding motor program. *Nature* **499**, 83–87 (2013).
12. A. Manzo, M. Silies, D. M. Gohl, K. Scott, Motor neurons controlling fluid ingestion in *Drosophila*. *Proc. Natl. Acad. Sci. U.S.A.* **109**, 6307–6312 (2012).
13. M. D. Gordon, K. Scott, Motor control in a *Drosophila* taste circuit. *Neuron* **61**, 373–384 (2009).
14. C. E. McKellar, Motor control of fly feeding. *J. Neurogenet.* **30**, 101–111 (2016).
15. A.-H. Pool, P. Kvello, K. Mann, S. K. Cheung, M. D. Gordon, L. Wang, K. Scott, Four GABAergic interneurons impose feeding restraint in *Drosophila*. *Neuron* **83**, 164–177 (2014).
16. R. F. Stocker, The organization of the chemosensory system in *Drosophila* melanogaster: A review. *Cell Tissue Res.* **275**, 3–26 (1994).
17. G. S. Pollack, Labellar lobe spreading in the blowfly: Regulation by taste and satiety. *J. Comp. Physiol.* **121**, 115–134 (1977).
18. N. C. Klapoetke, Y. Murata, S. S. Kim, S. R. Pulver, A. Birdsey-Benson, Y. K. Cho, T. K. Morimoto, A. S. Chuong, E. J. Carpenter, Z. Tian, J. Wang, Y. Xie, Z. Yan, Y. Zhang, B. Y. Chow, B. Surek, M. Melkonian, V. Jayaraman, M. Constantine-Paton, G. K.-S. Wong, E. S. Boyden, Independent optical excitation of distinct neural populations. *Nat. Methods* **11**, 338–346 (2014).
19. D.-G. Luo, W. W. S. Yue, P. Ala-Laurila, K.-W. Yau, Activation of visual pigments by light and heat. *Science* **332**, 1307–1312 (2011).
20. L.-H. Cao, B.-Y. Jing, D. Yang, X. Zeng, Y. Shen, Y. Tu, D.-G. Luo, Distinct signaling of *Drosophila* chemoreceptors in olfactory sensory neurons. *Proc. Natl. Acad. Sci. U.S.A.* **113**, E902–E911 (2016).
21. R. Falk, N. Bleiser-Avivi, J. Atidia, Labellar taste organs of *Drosophila melanogaster*. *J. Morphol.* **150**, 327–341 (1976).
22. S. E. Kim, B. Coste, A. Chadha, B. Cook, A. Patapoutian, The role of *Drosophila* Piezo in mechanical nociception. *Nature* **483**, 209–212 (2012).
23. P. Cameron, M. Hiroi, J. Ngai, K. Scott, The molecular basis for water taste in *Drosophila*. *Nature* **465**, 91–95 (2010).
24. D. A. Gorczyca, S. Younger, S. Meltzer, S. E. Kim, L. Cheng, W. Song, H. Y. Lee, L. Y. Jan, Y. N. Jan, Identification of Ppk26, a DEG/ENaC channel functioning with Ppk1 in a mutually dependent manner to guide locomotion behavior in *Drosophila*. *Cell Rep.* **9**, 1446–1458 (2014).
25. Z. Yan, W. Zhang, Y. He, D. Gorczyca, Y. Xiang, L. E. Cheng, S. Meltzer, L. Y. Jan, Y. N. Jan, *Drosophila* NOMPC is a mechanotransduction channel subunit for gentle-touch sensation. *Nature* **493**, 221–225 (2013).
26. W. D. Tracey Jr., R. I. Wilson, G. Laurent, S. Benzer, *painless*, a *Drosophila* gene essential for nociception. *Cell* **113**, 261–273 (2003).
27. Y. Guo, Y. Wang, Q. Wang, Z. Wang, The role of PPK26 in *Drosophila* larval mechanical nociception. *Cell Rep.* **9**, 1183–1190 (2014).
28. R. G. Walker, A. T. Willingham, C. S. Zuker, A *Drosophila* mechanosensory transduction channel. *Science* **287**, 2229–2234 (2000).
29. Z. Chen, Q. Wang, Z. Wang, The amiloride-sensitive epithelial Na^+ channel PPK28 is essential for drosophila gustatory water reception. *J. Neurosci.* **30**, 6247–6252 (2010).
30. L. E. Cheng, W. Song, L. L. Looger, L. Y. Jan, Y. N. Jan, The role of the TRP channel NompC in *Drosophila* larval and adult locomotion. *Neuron* **67**, 373–380 (2010).
31. M. C. Göpfert, J. T. Albert, B. Nadrowski, A. Kamikouchi, Specification of auditory sensitivity by *Drosophila* TRP channels. *Nat. Neurosci.* **9**, 999–1000 (2006).
32. B. P. Lehnert, A. E. Baker, Q. Gaudry, A.-S. Chiang, R. I. Wilson, Distinct roles of TRP channels in auditory transduction and amplification in *Drosophila*. *Neuron* **77**, 115–128 (2013).
33. T. Miyazaki, K. Ito, Neural architecture of the primary gustatory center of *Drosophila melanogaster* visualized with GAL4 and LexA enhancer-trap systems. *J. Comp. Neurol.* **518**, 4147–4181 (2010).
34. W. Fischler, P. Kong, S. Marella, K. Scott, The detection of carbonation by the Drosophila gustatory system. *Nature* **448**, 1054–1057 (2007).
35. O. Schwarz, A. A. Bohra, X. Liu, H. Reichert, K. VijayRaghavan, J. Pielage, Motor control of *Drosophila* feeding behavior. *eLife* **6**, e19892 (2017).

36. E. H. Feinberg, M. K. VanHoven, A. Bendesky, G. Wang, R. D. Fetter, K. Shen, C. I. Bargmann, GFP reconstitution across synaptic partners (GRASP) defines cell contacts and synapses in living nervous systems. *Neuron* **57**, 353–363 (2008).
37. K. Wang, J. Gong, Q. Wang, H. Li, Q. Cheng, Y. Liu, S. Zeng, Z. Wang, Parallel pathways convey olfactory information with opposite polarities in *Drosophila*. *Proc. Natl. Acad. Sci. U.S.A.* **111**, 3164–3169 (2014).
38. T. Effertz, R. Wiek, M. C. Göpfert, NompC TRP channel is essential for *Drosophila* sound receptor function. *Curr. Biol.* **21**, 592–597 (2011).
39. D. F. Eberl, R. W. Hardy, M. J. Kernan, Genetically similar transduction mechanisms for touch and hearing in *Drosophila*. *J. Neurosci.* **20**, 5981–5988 (2000).
40. J. Li, W. Zhang, Z. Guo, S. Wu, L. Y. Jan, Y.-N. Jan, A defensive kicking behavior in response to mechanical stimuli mediated by *Drosophila* wing margin bristles. *J. Neurosci.* **36**, 11275–11282 (2016).

Acknowledgments: We thank W. W. S. Yue, Z. Wang, W. Zhang, M. Luo, and Y. Zhong for discussions or comments on the manuscript. We also thank Y. Hu, Y. Liu, Y. Jiang, and X. Hao of the Imaging Core Facility, X. Xu and W. Yang for behavioral quantification, and B. Deng for trichromatic confocal imaging. **Funding:** This work was supported by National Natural Science Foundation of China (31471053, 31671085, and 31871058), the Ministry of Education [the Young Thousand Talent Program (to D.-G. L.)], and the State Key Laboratory of Membrane Biology. **Author contributions:** L.-H.C. and D.-G.L. conceived the study. Y.Z., L.-H.C., and D.-G.L. designed the experiments. Y.Z. performed electrophysiological recordings under the guidance of L.-H.C. and performed GRASP experiments. Y.Z. performed the electron microscopy experiments with help from the Imaging Core Facility (College of Life Sciences, Peking University). X.-W.S. and X.-Q.G. performed the behavioral experiments and immunostaining. L.-H.C., Y.Z., and D.-G.L. analyzed the data. L.-H.C., Y.Z., and D.-G.L. wrote the manuscript. **Competing interests:** The authors declare that they have no competing interests. **Data and materials availability:** All data needed to evaluate the conclusions in the paper are present in the paper and/or the Supplementary Materials. Additional data related to this paper may be requested from the authors.

Submitted 31 December 2018
Accepted 17 April 2019
Published 22 May 2019
10.1126/sciadv.aaw5141

Citation: Y. Zhou, L.-H. Cao, X.-W. Sui, X.-Q. Guo, D.-G. Luo, Mechanosensory circuits coordinate two opposing motor actions in *Drosophila* feeding. *Sci. Adv.* **5**, eaaw5141 (2019).